Electronic Supplementary Information

Controllable Inverse C_2H_2/CO_2 Separation in Ultra-Stable Zn-Organic Frameworks for Efficient Removal of Trace CO_2 from Acetylene

Jia Yu, Jing Zhang, Peng Zhang*, Ying Wang, Shu-Ni Li, Quan-Guo Zhai*

Key Laboratory of Macromolecular Science of Shaanxi Province, School of Chemistry & Chemical Engineering, Shaanxi Normal University, Xi'an, Shaanxi, 710062, China.

*Corresponding authors

E-mail: peng.zhang@snnu.edu.cn, zhaiqg@snnu.edu.cn.

Table S1. Crystal data and structure refinements for SNNU-334-336.

MOF	**SNNU-334**	**SNNU-335**	**SNNU-336**
Empirical formula	$C_{58}H_{34}N_8O_{12}Zn_3$	$C_{60}H_{42}N_{12}O_{12}Zn_3$	$C_{60}H_{36}N_6O_{12}Zn_3$
Formula weight	1231.04	1319.24	1229.15
Crystal system	Cubic	Cubic	Cubic
Space group	*Pa*-3	*Pa*-3	*Pa*-3
a(Å)	23.620(2)	23.978(2)	23.941(2)
b(Å)	23.620(2)	23.978(2)	23.941(2)
c(Å)	23.620(9)	23.978(2)	23.941(2)
α(deg)	90	90	90
β(deg)	90	90	90
γ(deg)	90	90	90
Volume (Å^3)	13177.7(19)	13786(2)	13722.5(2)
Z	8	24	24
$d_{calcd.}$ (g·m^{-3})	1.241	1.2711	1.1898
Wavelength	0.71073 Å	0.71073 Å	0.71073 Å
F(000)	4992	4992	4992
R_{int}	0.1165	0.0465	0.0669
Reflections collected/unique	65062/3891	440377/4685	438629/4679
Data/restraints/parameters	3891/9/261	4685/0/263	4679/0/244
GOF on F^2	1.036	1.445	1.142
R_1[a], wR_2[b][$I > 2\sigma(I)$]	0.056, 0.1460	0.0857, 0.2941	0.0436, 0.1454
R_1[a], wR_2[b] (all data)	0.1261, 01334	0.0866, 0.2823	0.046, 0.143

[a] $R_1 = \sum(|F_o|-|F_c|)/\sum|F_o|$, $wR_2 = [\sum w(F_o^2-F_c^2)2/\sum w(F_o^2)^2]^{0.5}$

Table S2. Selected bond lengths (Å) and bond angles (°) of SNNU-334-336.

SNNU-334		**SNNU-335**		**SNNU-336**	
Zn1-N1	2.014(4)	Zn1-N1	2.037(3)	Zn1-N1	2.035(2)
Zn1-N3	2.012(4)	Zn1-N2	2.040(3)	Zn1-N2	2.037(2)
Zn1-O1	1.914(3)	Zn1-O1	1.947(3)	Zn1-O1	1.9399(19)
Zn1-O3	1.900(4)	Zn1-O3	1.956(3)	Zn1-O3	1.9533(19)
O1-Zn1-O3	106.06(18)	O1-Zn1-O3	103.61(14)	O1-Zn1-O3	105.13(9)
N1-Zn1-N3	107.28(19)	N1-Zn1-N2	109.01(14)	N1-Zn1-N2	109.31(9)
O1-Zn1-N1	114.54(17)	O1-Zn1-N1	96.41(14)	O1-Zn1-N1	97.54(9)
O1-Zn1-N3	113.88(18)	O1-Zn1-N2	117.68(14)	O1-Zn1-N2	116.61(9)
O3-Zn1-N1	116.8(2)	O3-Zn1-N1	112.81(14)	O3-Zn1-N1	112.89(9)
O3-Zn1-N3	97.2(2)	O3-Zn1-N2	115.77(14)	O3-Zn1-N2	114.25(9)
C15-O1-Zn1	108.3(4)	C15-O1-Zn1	123.9(3)	C15-O3-Zn1	107.57(18)
C18-O3-Zn1	124.3(5)	C18-O3-Zn1	106.8(3)	C18-O1-Zn1	124.42(18)
C1-N1-Zn1	122.9(4)	C1-N1-Zn1	123.3(3)	C1-N2-Zn1	119.96(18)
C3-N8-Zn1	118.8(5)	C5-N1-Zn1	119.7(2)	C5-N2-Zn1	121.62(19)
C5-N1-Zn1	119.8(4)	C8-N2-Zn1	122.3(3)	C8-N1-Zn1	123.70(18)
C8’-N3-Zn1	118.7(14)	C12-N2-Zn1	119.7(3)	C12-N1-Zn1	118.60(18)
C12-N3-Zn1	125.2(5)				
C12’-N3-Zn1	127.9(14)				

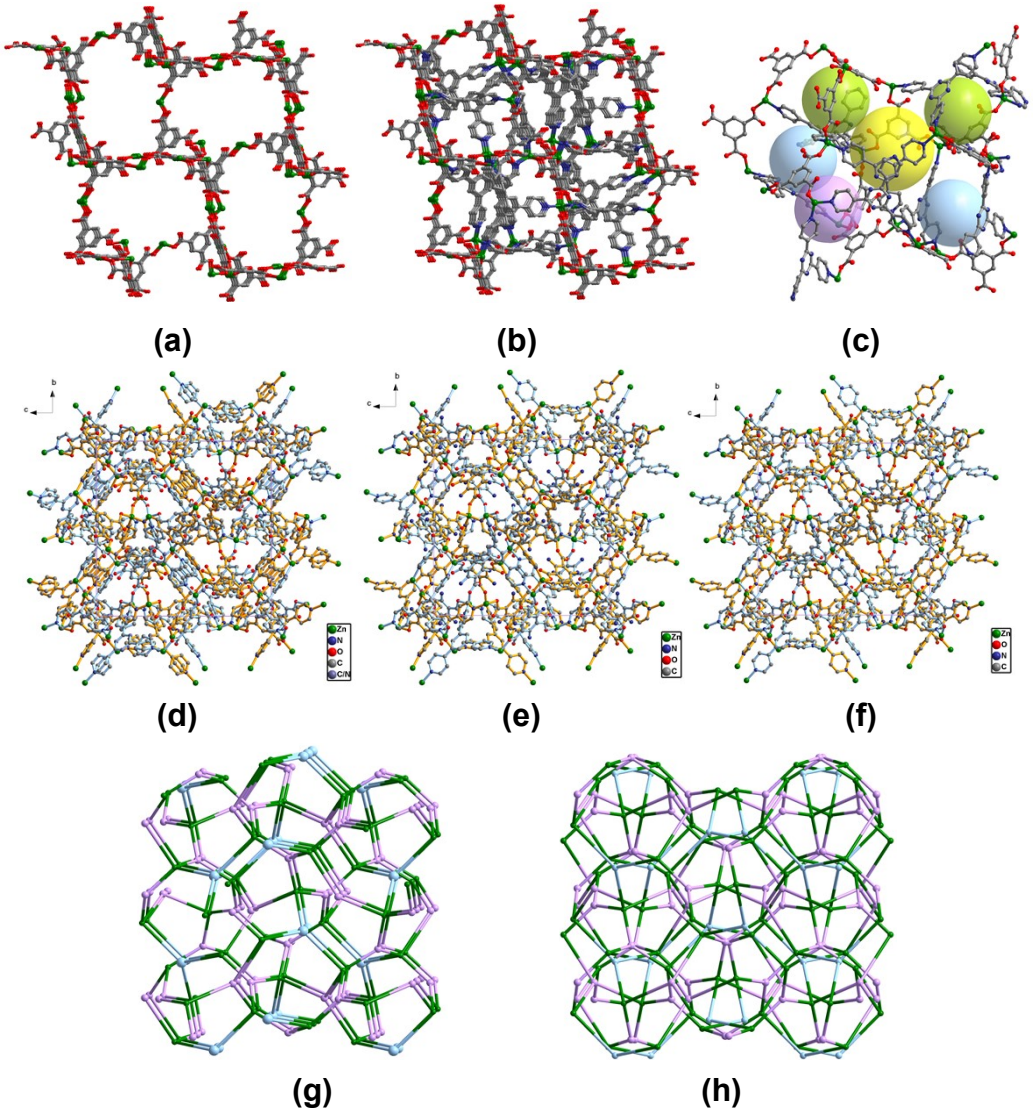

Figure S1. (a) The structure generated by Zn^{2+} and BTC ligands in SNNU-334-336. (b) The 3D framework formed by the further coordination with tri-pyridine ligands. (c) The linkage between four types of metal-organic cages. (d-f) The 2-fold interpenetrated frameworks of SNNU-334-336 viewed along the a-axis direction. (g and h) The topological representations for the single and 2-fold interpenetrated metal-organic frameworks.

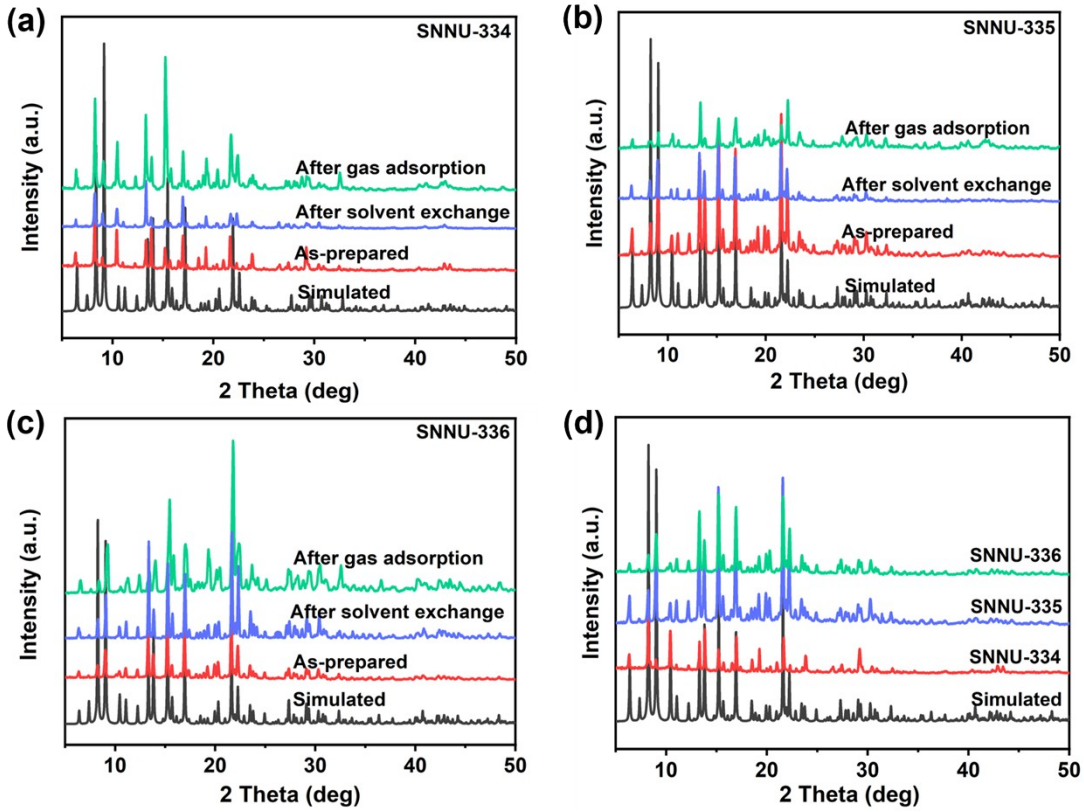

Figure S2. PXRD patterns of SNNU-334-336.

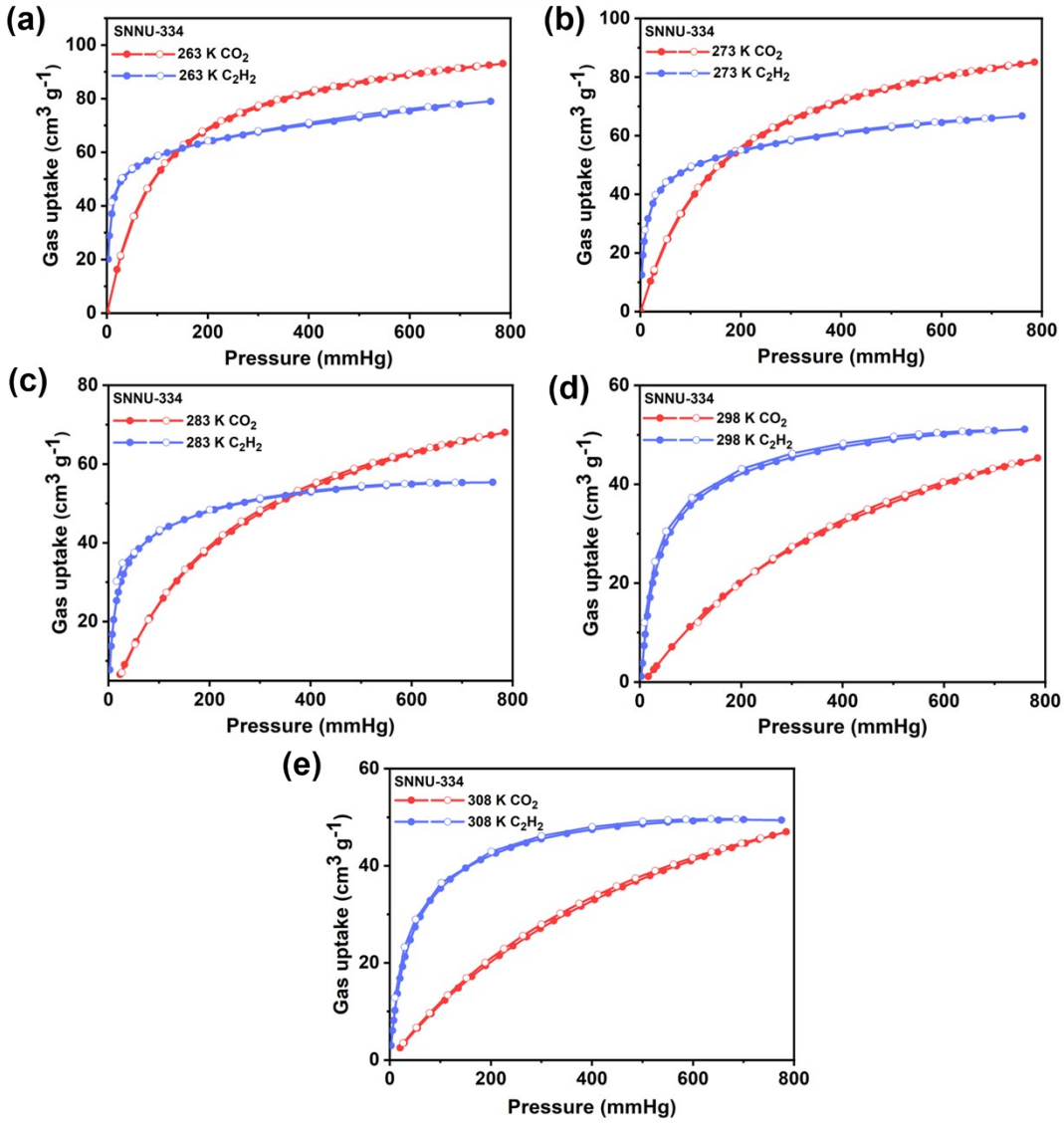

Figure S3. The adsorption curves of CO_2 and C_2H_2 for SNNU-334 at 263 K-308 K.

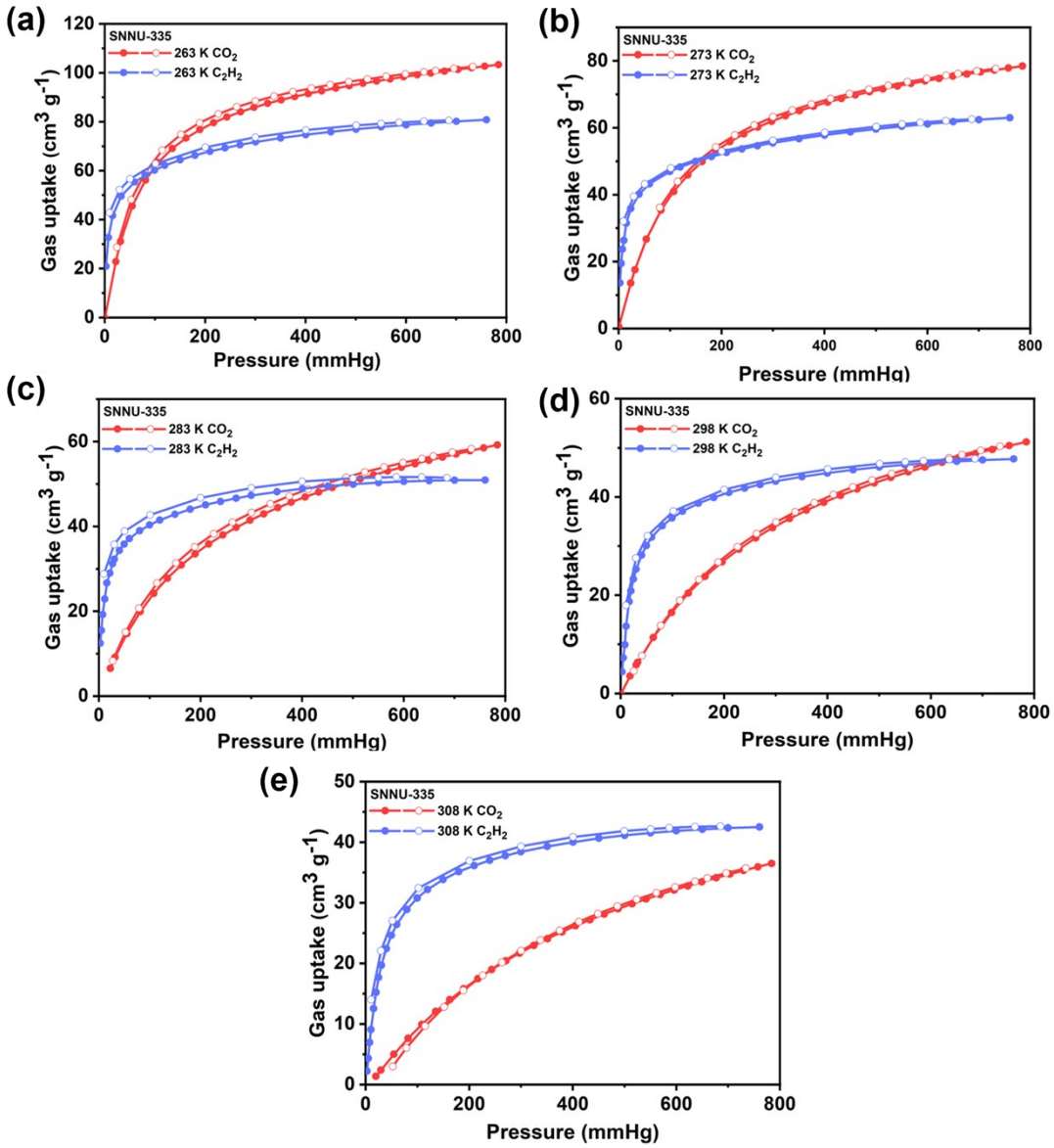

Figure S4. The adsorption curves of CO_2 and C_2H_2 for SNNU-335 at 263 K-308 K.

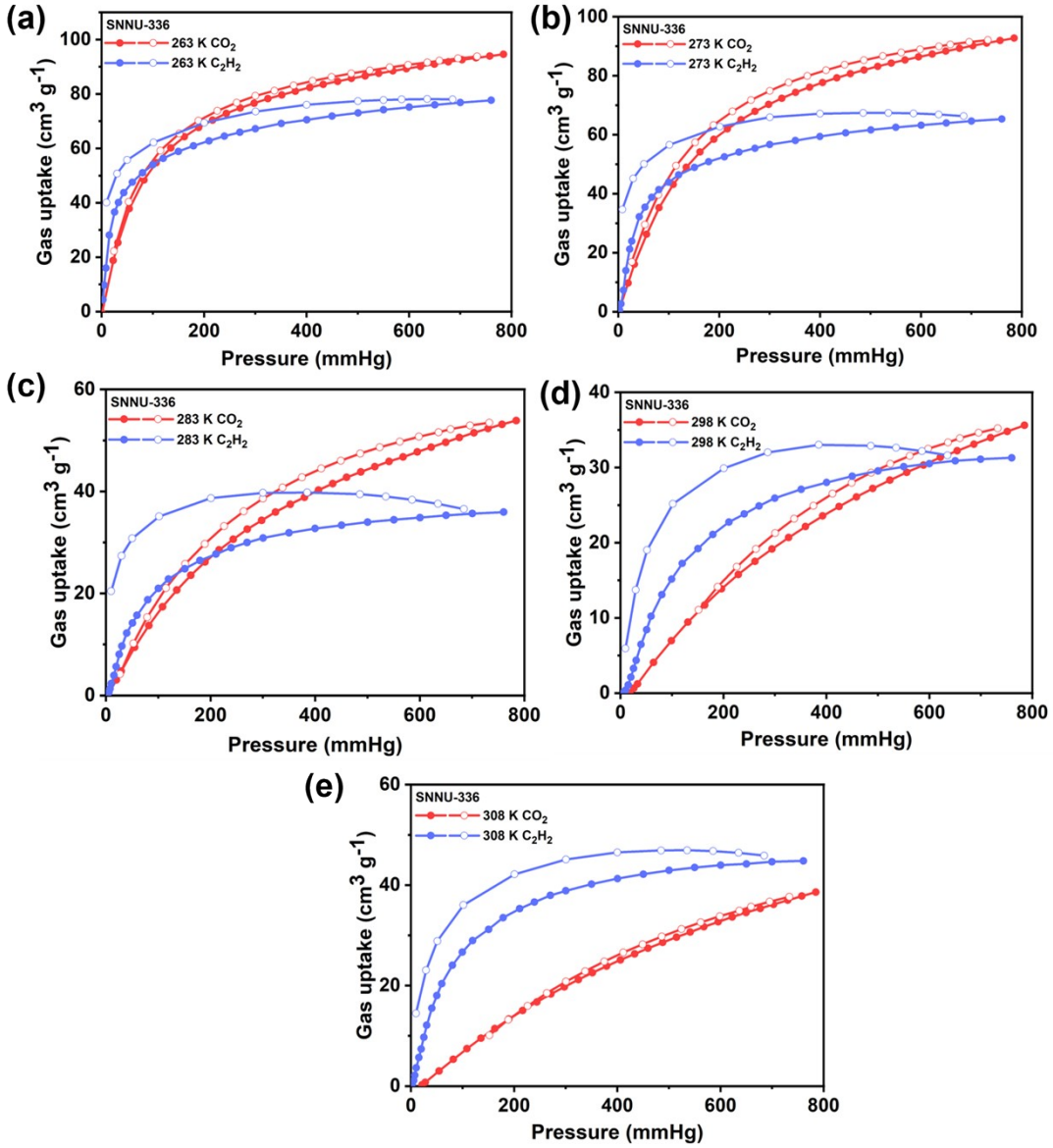

Figure S5. The adsorption curves of CO_2 and C_2H_2 for SNNU-336 at 263 K-308 K.

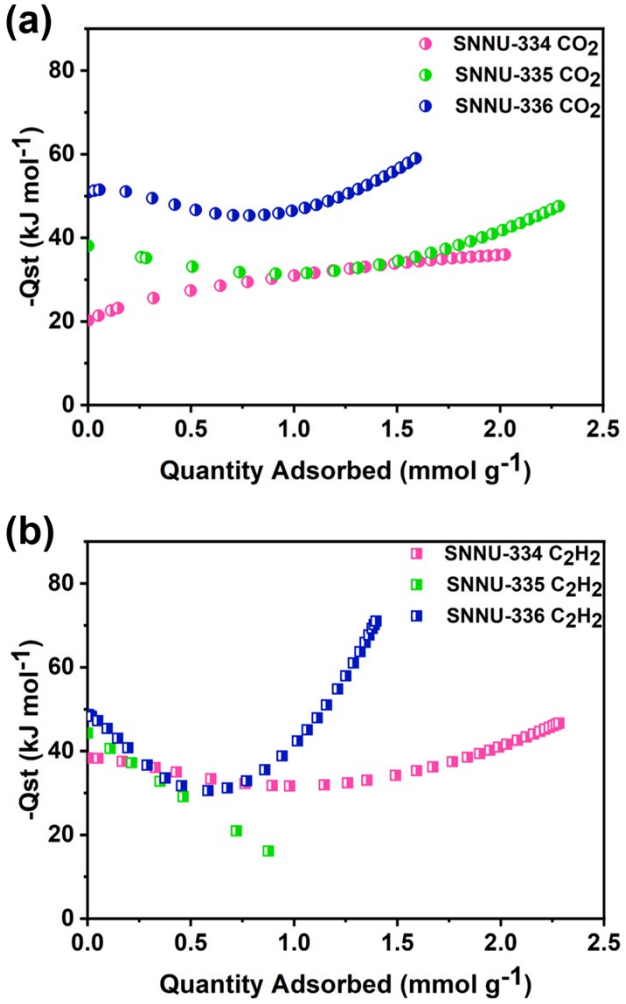

Figure S6. The calculated Q_{st} values for SNNU-334-336 of CO_2 (a) and C_2H_2 (b).

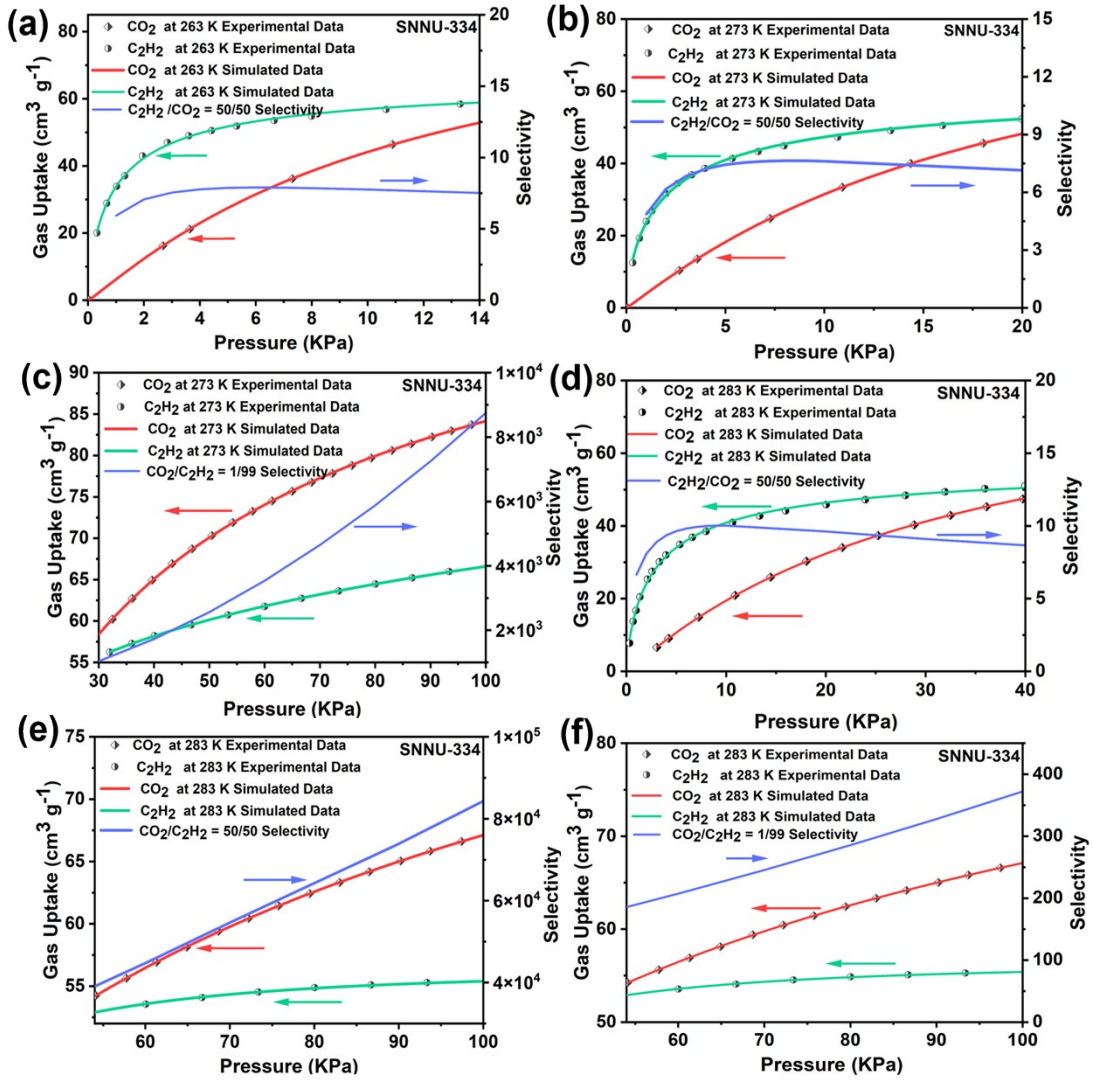

Figure S7. IAST selectivity data for SNNU-334: (a) C_2H_2/CO_2 = 50/50 before reverse point at 263 K; (b) C_2H_2/CO_2 = 50/50 before reverse point 273 K; (c) CO_2/C_2H_2 = 1/99 at 273 K after reverse point; (d) C_2H_2/CO_2 = 50/50 at 283 K before reverse point; (e) CO_2/C_2H_2 = 50/50 after reverse point; (f) CO_2/C_2H_2 = 1/99 at 283 K after reverse point.

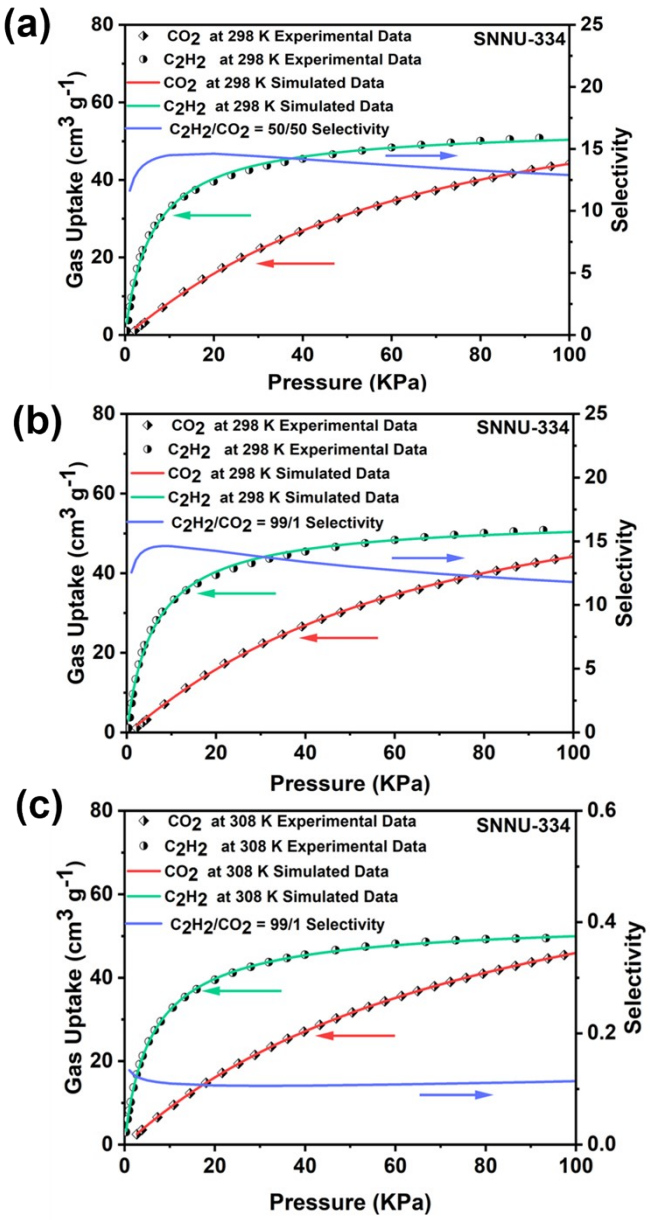

Figure S8. IAST selectivity data for SNNU-334: (a) C_2H_2/CO_2 = 50/50 at 298 K; (b) C_2H_2/CO_2 = 1/99 at 298 K; (c) C_2H_2/CO_2 = 1/99 at 308 K.

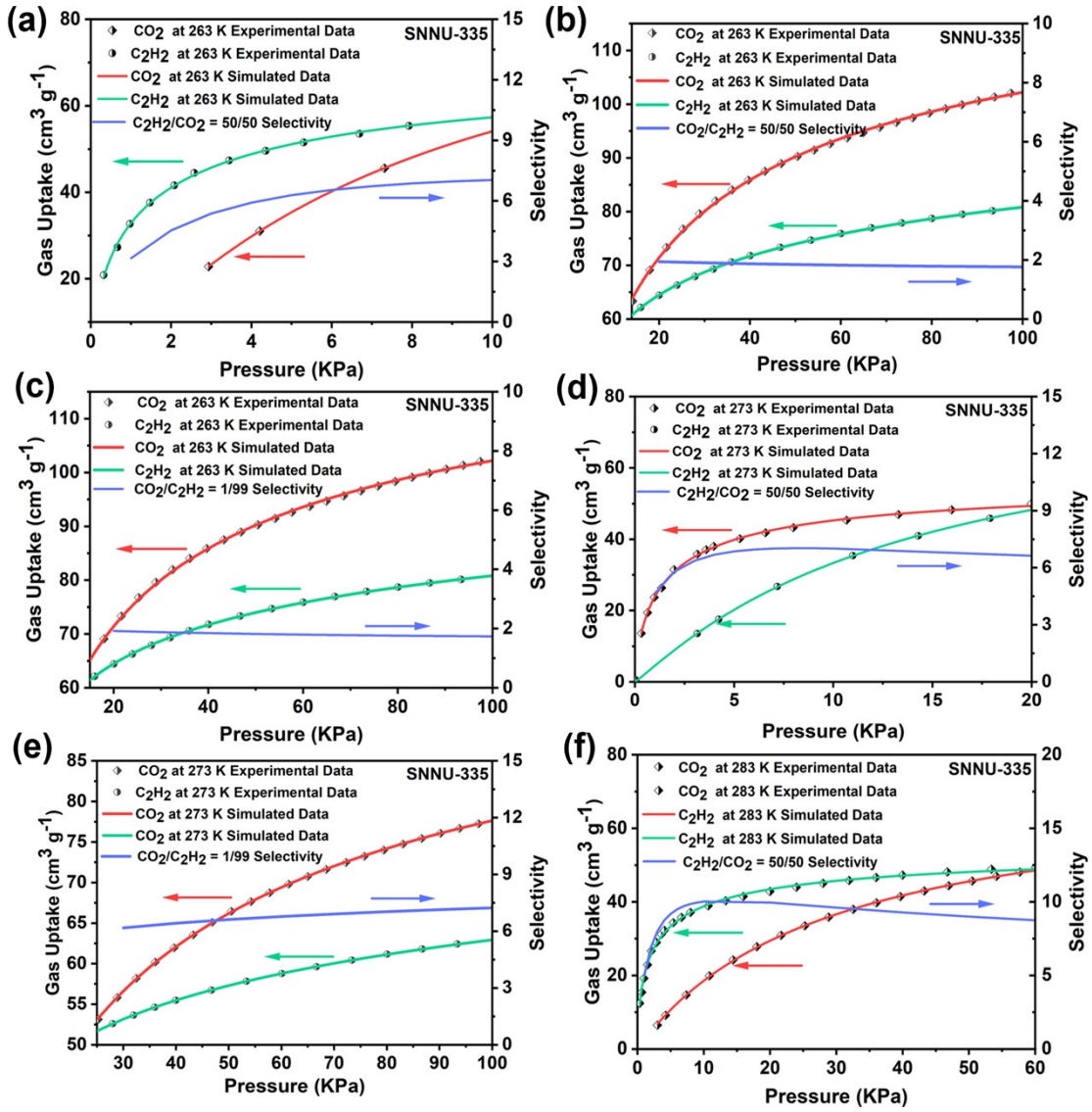

Figure S9. IAST selectivity data for SNNU-335: (a) C_2H_2/CO_2 = 50/50 before reverse point at 263 K; (b) C_2H_2/CO_2 = 50/50 after reverse point at 263 K; (c) CO_2/C_2H_2 = 1/99 after reverse point at 273 K; (d) C_2H_2/CO_2 = 50/50 before reverse point at 273 K; (e) CO_2/C_2H_2 =1/99 after reverse point at 273 K; (f) C_2H_2/CO_2=50/50 before reverse point at 283 K.

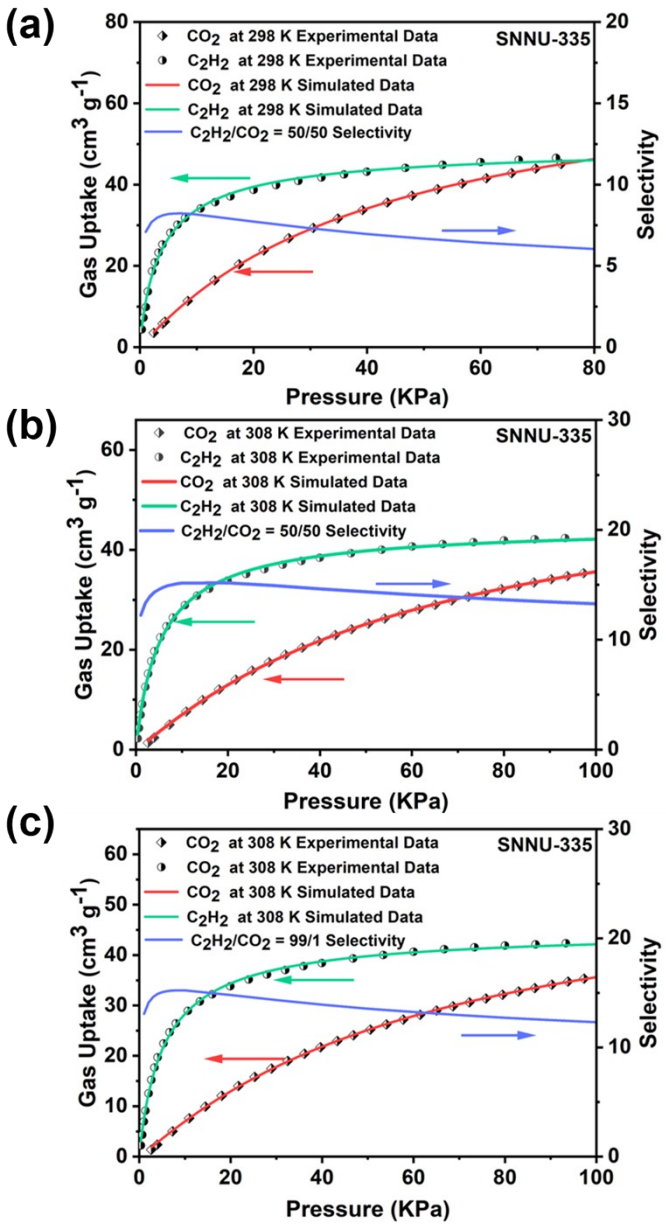

Figure S10. IAST selectivity data for SNNU-335: (a) C_2H_2/CO_2 = 50/50 at 298 K; (b) C_2H_2/CO_2 = 50/50 at 308 K; (c) C_2H_2/CO_2 = 99/1 at 308 K.

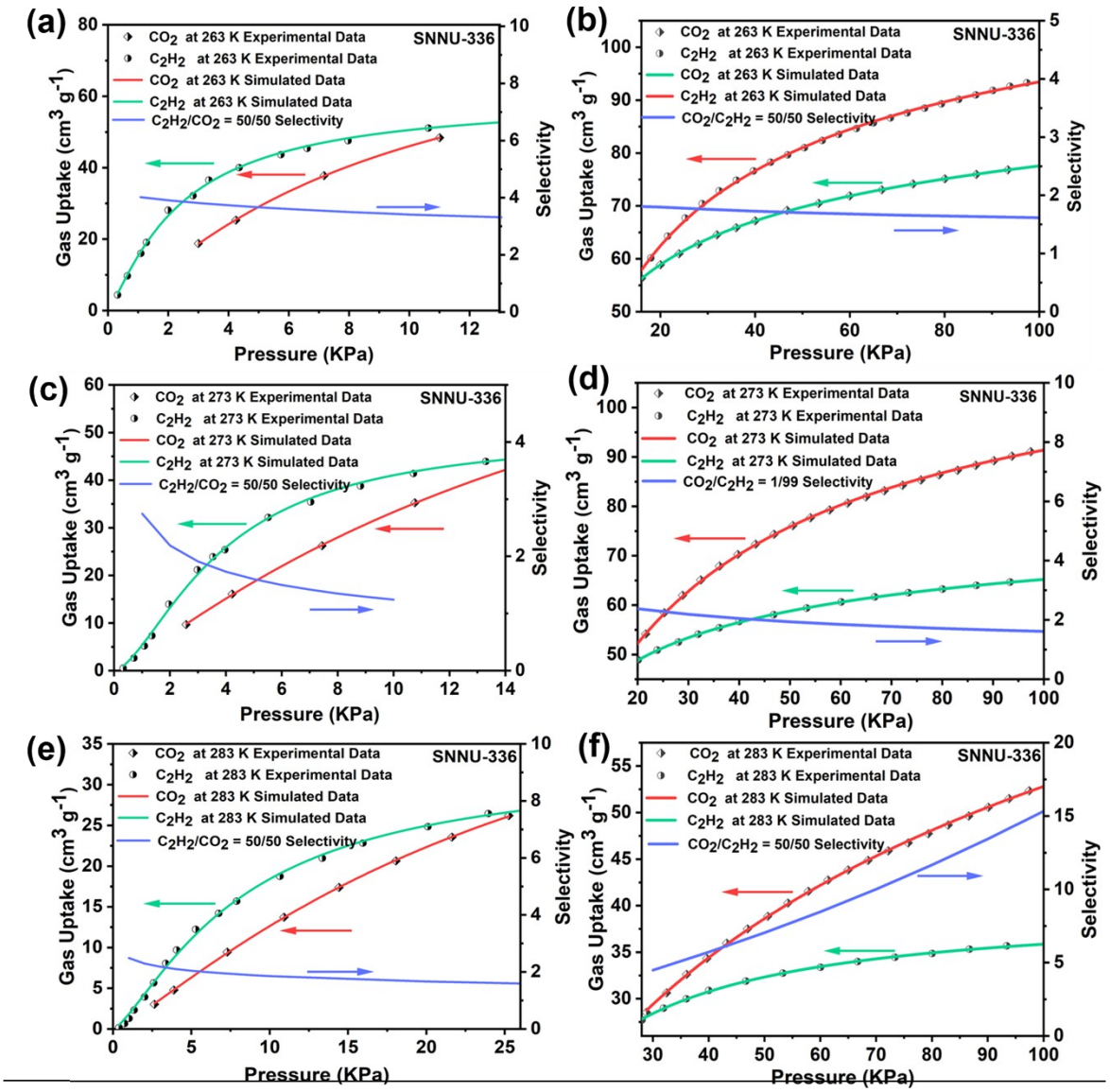

Figure S11. IAST selectivity data for SNNU-336: (a) C_2H_2/CO_2=50/50 before reverse point at 263 K; (b) CO_2/C_2H_2 = 50/50 after reverse point at 263 K; (c) C_2H_2/CO_2 = 50/50 before reverse point at 273 K; (d) CO_2/C_2H_2 = 1/99 after reverse point at 273 K; (e) C_2H_2/CO_2 = 50/50 before reverse point at 283 K; (f) CO_2/C_2H_2 = 50/50 after reverse point at 283 K.

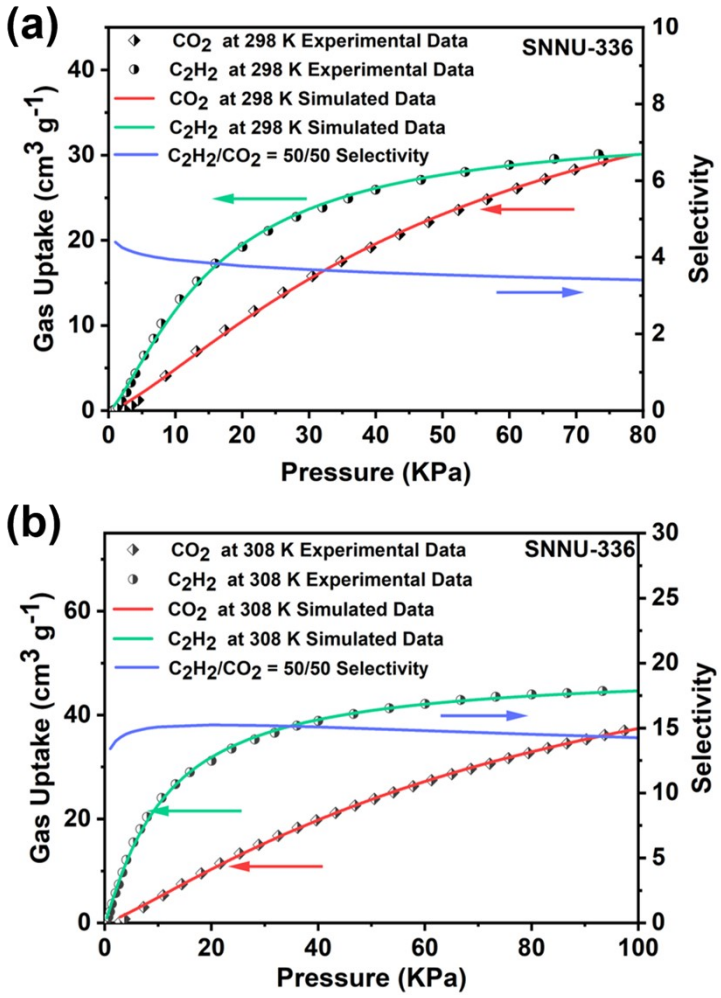

Figure S12. IAST selectivity data for SNNU-336: C_2H_2/CO_2 = 50/50 at 298 K (a) and 308 K (b).

Breakthrough Experiments and Procedures

The breakthrough experiments are carried out in a dynamic equipment, which is built in cooperation with the instrument supplier (Xi′an Sirius Scientific Research Instrument Co., Ltd.). The activated MOF samples (SNNU-334: 730.5 mg; SNNU-335: 546.3 mg; SNNU-336: 780.0 mg) were loaded into a stainless-steel column with an inradium of about 4 mm, and both ends were sealed with absorbent cotton. The column was placed in a circulating catheter sleeve connected to a thermostatic bath (temperature range from 263 K to 298 K). The flow and pressure of the mixed gas are controlled by the pressure control valve and the mass flow controller, respectively. Outlet effluent was continuously monitored using a mass spectrometer (Hiden, HPR-20) or gas chromatography (Fuli Instruments, 9790II). Before the start of each breakthrough experiment, the sample column was purged with He flow (30 mL min^{-1}) for 3-5 h to further activate the sample.

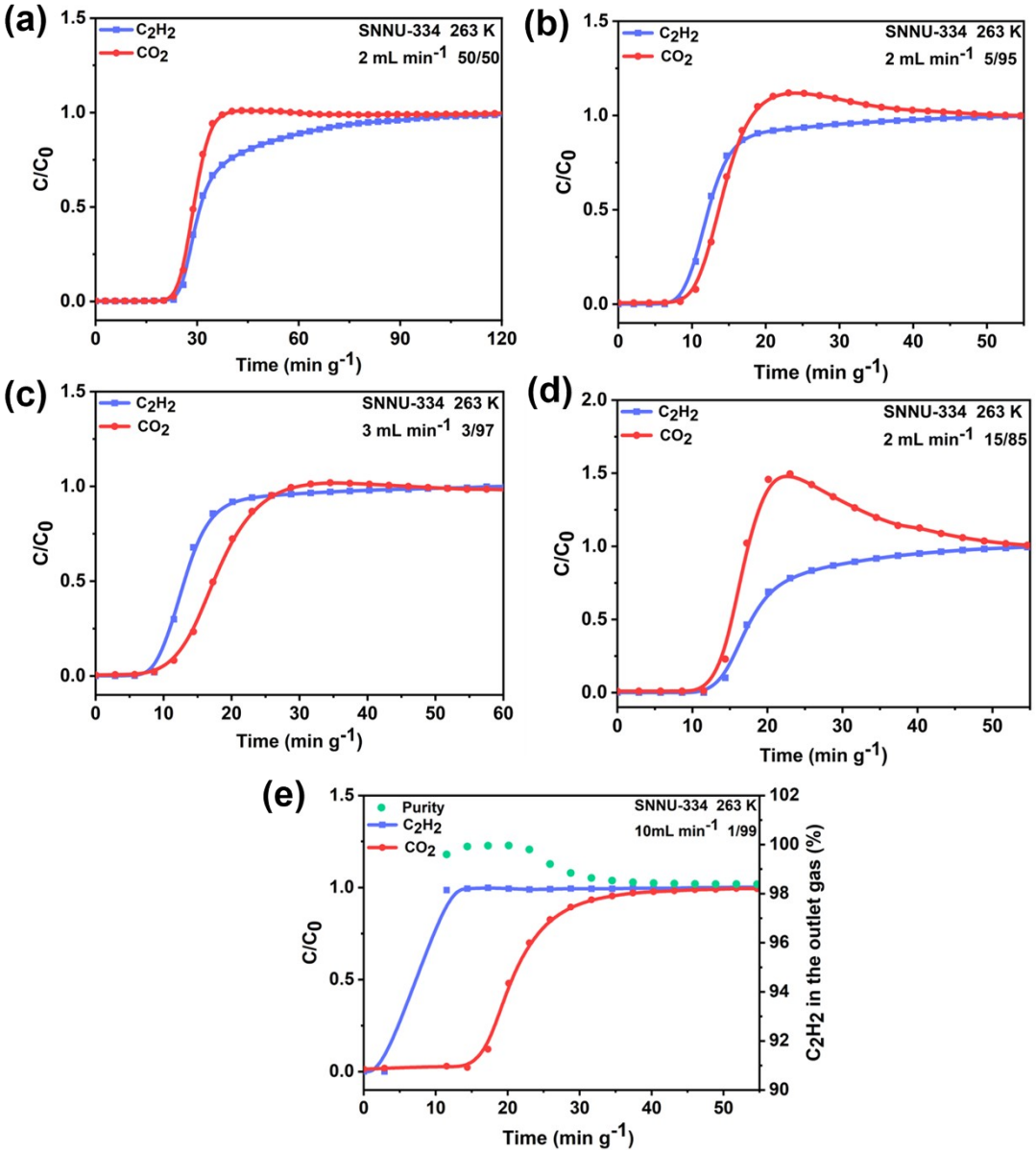

Figure S13. Experimental breakthrough curves of SNNU-334 at 263 K: (a) CO_2/C_2H_2 = 50/50; (b) CO_2/C_2H_2 = 5/95; (c) CO_2/C_2H_2 = 3/97; (d) CO_2/C_2H_2 = 15/85; (e) CO_2/C_2H_2 = 1/99.

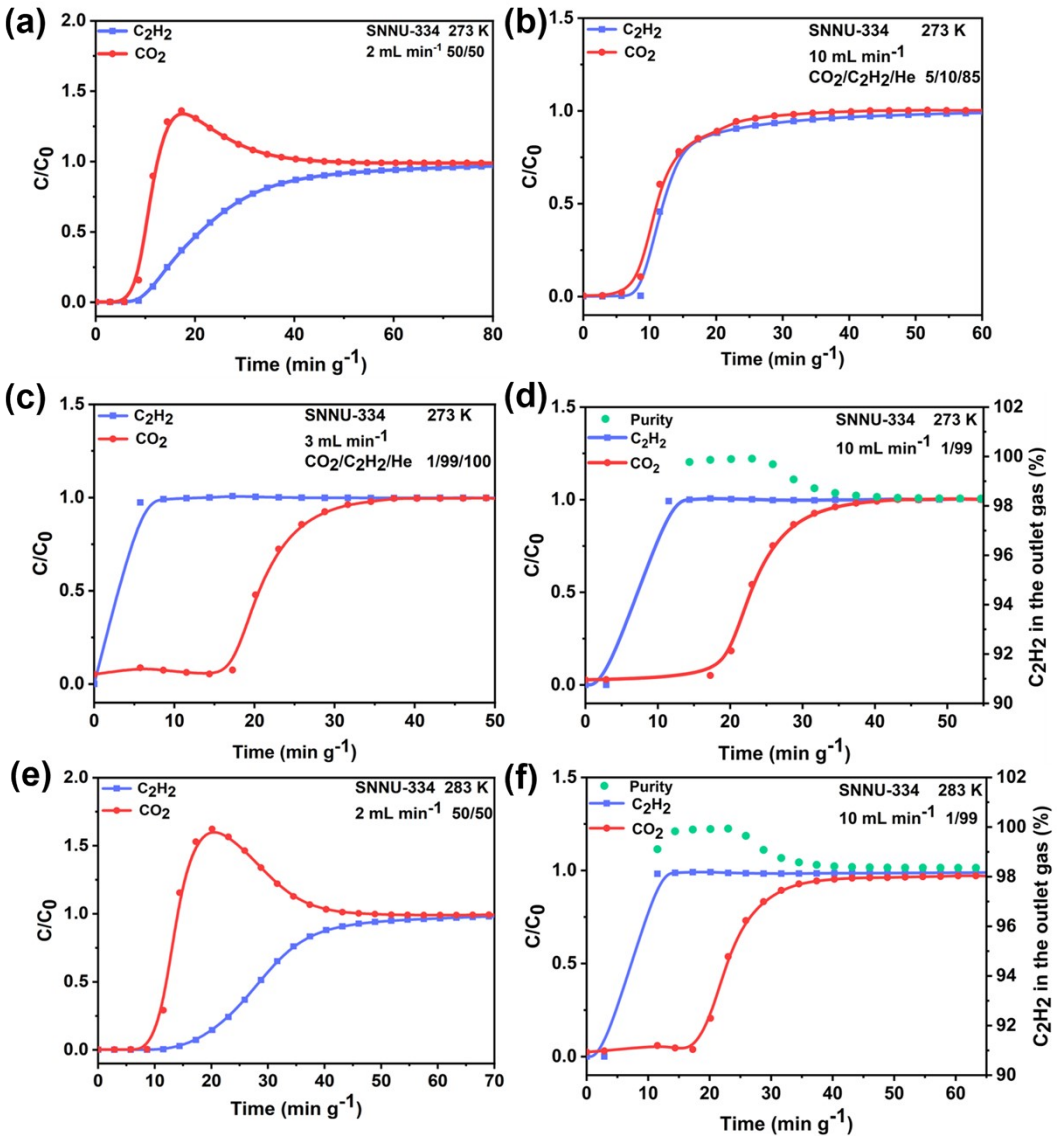

Figure S14. Experimental breakthrough curves of SNNU-334: (a) CO_2/C_2H_2 = 50/50; (b) CO_2/C_2H_2/He = 5/10/85; (c) CO_2/C_2H_2/He = 1/99/100; (d) CO_2/C_2H_2 = 1/99 at 273 K; (e) CO_2/C_2H_2 = 50/50; (f) CO_2/C_2H_2 = 1/99 at 283 K.

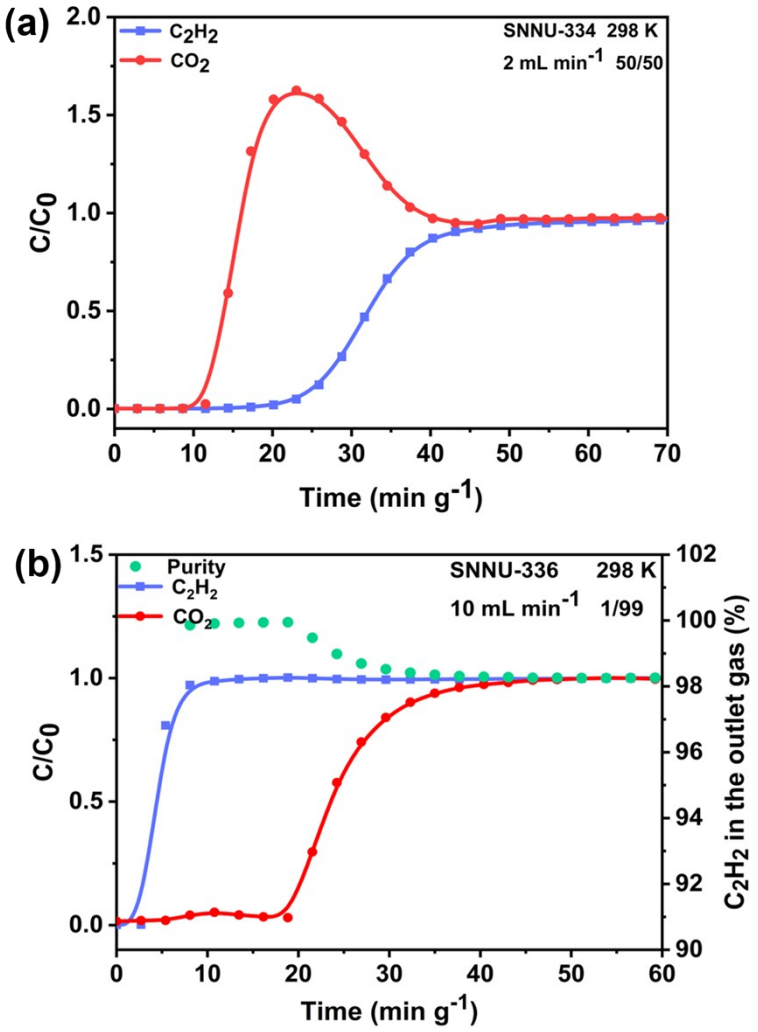

Figure S15. Experimental breakthrough curves of SNNU-334: (a) CO_2/C_2H_2 = 50/50 and (b) CO_2/C_2H_2 = 1/99 at 298 K.

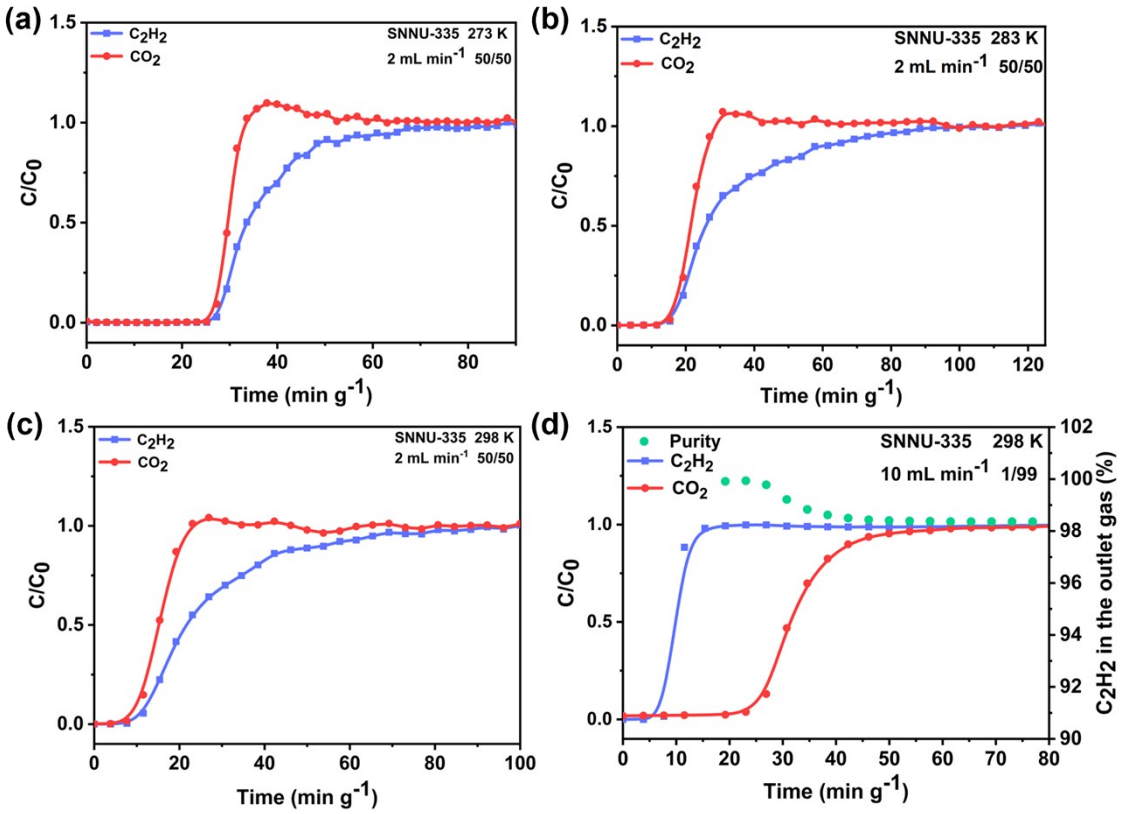

Figure S16. Experimental breakthrough curves of SNNU-335: (a) CO_2/C_2H_2 = 50/50 at 273 K; (b) CO_2/C_2H_2 = 50/50 at 283 K; (c) CO_2/C_2H_2 = 50/50 at 298 K; (d) CO_2/C_2H_2 = 1/99 at 298 K.

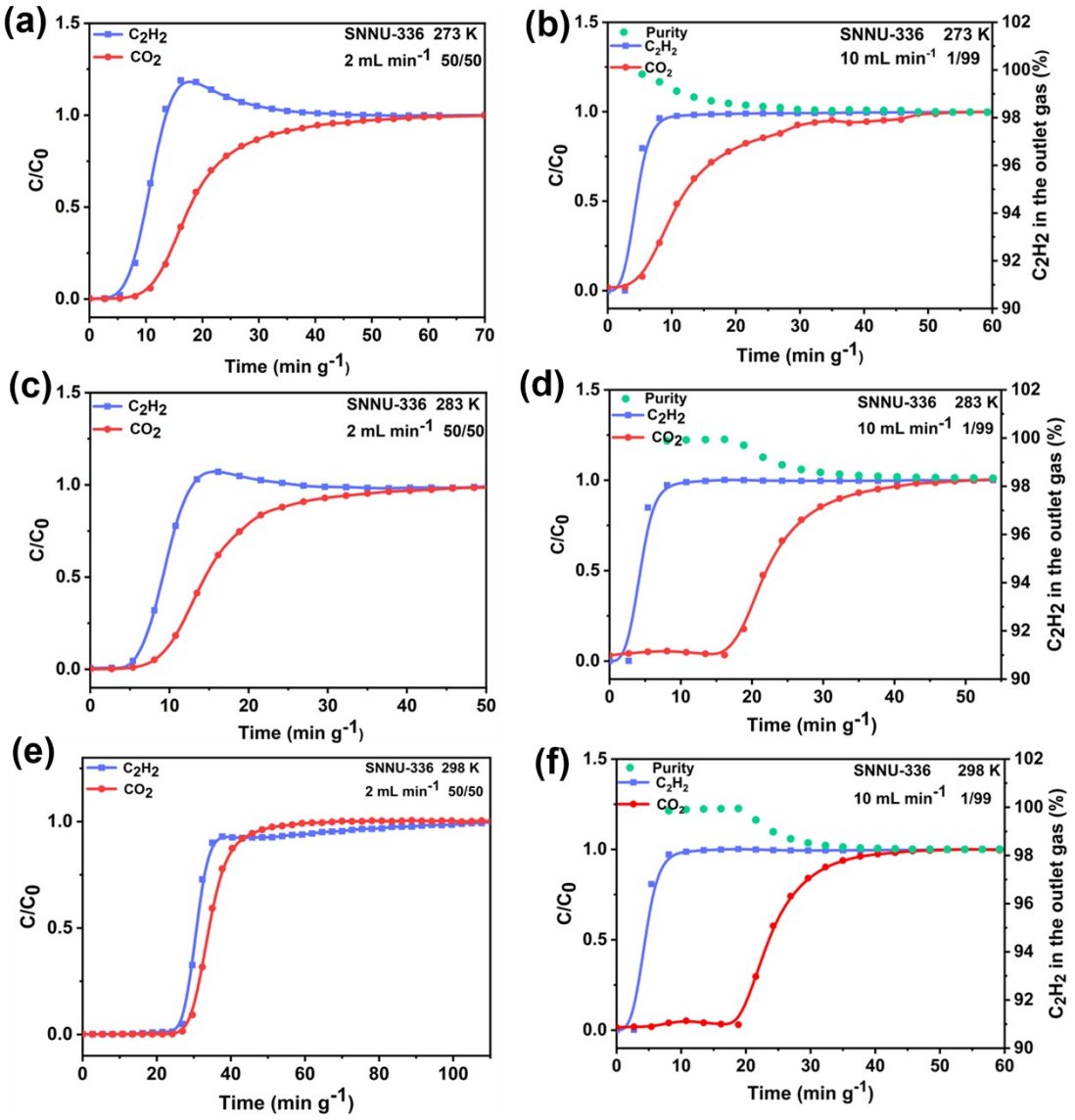

Figure S17. Experimental breakthrough curves of SNNU-336: (a) CO_2/C_2H_2 = 50/50 at 273 K; (b) CO_2/C_2H_2 = 1/99 at 273 K; (c) CO_2/C_2H_2 = 50/50 at 283 K; (d) CO_2/C_2H_2 = 1/99 at 283 K; (e) CO_2/C_2H_2 = 50/50 at 298 K; (f) CO_2/C_2H_2 = 1/99 at 298 K.

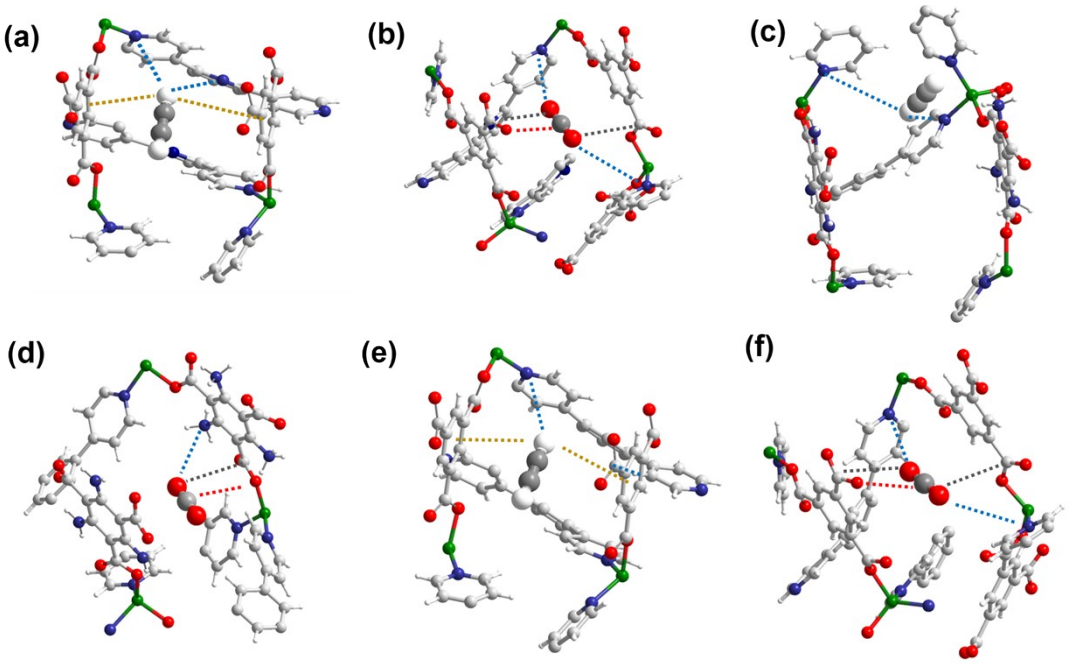

Figure S18. GCMC simulation of interactions between the MOF framework and gas molecule: C_2H_2 in SNNU-334-336 (a, c, and e) and CO_2 in SNNU-334-336 (b, d, f).

Table S3. Summary of CO_2 and C_2H_2 uptake capacity and the IAST CO_2/C_2H_2 selectivity for MOF adsorbents with inverse C_2H_2/CO_2 separation performance.

MOFs	CO_2/C_2H_2 IAST Selectivity (50/50)	CO_2 Uptake Capacity ($cm^3\ g^{-1}$)	C_2H_2 Uptake Capacity ($cm^3\ g^{-1}$)	Reference
Cu-F-pymo	>10[5a]	26.6	2.3	S1
SNNU-334	**3595.4[b]**	**85.1**	**66.8**	**This Work**
PMOF-1	694[b]	53.3	7.5	S2
MUF-16	510[c]	47.8	4.0	S3
Cd-NP	86[a]	58	9.7	S4
Ce-MIL-140-4F	40[b]	151.7	53.5	S5
$[Tm_2(OH\text{-}BDC)_2(\mu_3\text{-}OH)_2](H_2O)_2$	18.2[a]	130.6	47.0	S6
Mn(bdc)(dpe)	9.0[c]	45.9	7.3	S7
SIFSIX-3-Ni	7.5[a]	62.7	73.9	S8
SNNU-335	**6.9[b]**	**78.4**	**63.0**	**This Work**
PCP-NH_2-ipa	6.4[a]	72	43.4	S9
CD-MOF-2	6.1[a]	59.8	45.5	S10
PCP-NH_2-bdc	4.4[a]	68	42.7	S9
$K_2[Cr_3O(OOCH)_6]$	5.6[d]	11.2	2.4	S11
CD-MOF-1	3.4[a]	64.3	49.9	S10
$[Zn(atz)(BDC\text{-}Cl_4)_{0.5}]_n$	2.4[e]	34.6	18	S12
SNNU-336	**1.7[b]**	**92.7**	**65.3**	**This Work**
$[Tm_2(OH\text{-}BDC)_2(\mu_3\text{-}OH)_2]$	1.6[a]	139.1	117.6	S6

IAST selectivity for equimolar mixture: a-298 K, 101 KPa; b-273 K, 101 KPa; c-293 K, 101 KPa; d-273 K, 91 KPa; 293 K, 101 KPa; e-285 K, 101 KPa.

References

S1. Y. Shi, Y. Xie, H. Cui, Y. Ye, H. Wu, W. Zhou, H. Arman, R. B. Lin and B. Chen, *Adv. Mater.*, 2021, **33**, e2105880.

S2. L. Z. Cai, Z. Z. Yao, S. J. Lin, M. S. Wang and G. C. Guo, *Angew. Chem. Int. Ed.*, 2021, **60**, 18223-18230.

S3. O. T. Qazvini, R. Babarao and S. G. Telfer, *Nat*. *Commun.*, 2021, **12**, 197.

S4. Y. Xie, H. Cui, H. Wu, R. B. Lin, W. Zhou and B. Chen, *Angew. Chem. Int. Ed.*, 2021, **60**, 9604-9609.

S5. Z. Zhang, S. B. Peh, R. Krishna, C. Kang, K. Chai, Y. Wang, D. Shi and D. Zhao, *Angew. Chem. Int. Ed.*, 2021, **60**, 17198-17204.

S6. D. Ma, Z. Li, J. Zhu, Y. Zhou, L. Chen, X. Mai, M. Liufu, Y. Wu and Y. Li, *J. Mater. Chem. A*, 2020, **8**, 11933-11937.

S7. M. L. Foo, R. Matsuda, Y. Hijikata, R. Krishna, H. Sato, S. Horike, A. Hori, J. Duan, Y. Sato, Y. Kubota, M. Takata and S. Kitagawa, *J. Am. Chem. Soc.*, 2016, **138**, 3022-3030.

S8. K.-J. Chen, Hayley S. Scott, David G. Madden, T. Pham, A. Kumar, A. Bajpai, M. Lusi, Katherine A. Forrest, B. Space, John J. Perry and Michael J. Zaworotko, *Chem.*, 2016, **1**, 753-765.

S9. Y. Gu, J.-J. Zheng, K.-i. Otake, M. Shivanna, S. Sakaki, H. Yoshino, M. Ohba, S. Kawaguchi, Y. Wang, F. Li and S. Kitagawa, *Angew. Chem. Int. Ed.*, 2021, **60**, 11688-11694.

S10. L. Li, J. Wang, Z. Zhang, Q. Yang, Y. Yang, B. Su, Z. Bao and Q. Ren, *ACS. Appl. Mater. Interfaces*, 2019, **11**, 2543-2550.

S11. R. Eguchi, S. Uchida and N. Mizuno, *Angew. Chem. Int. Ed.*, 2012, **51**, 1635-1639.

S12. X.-Y. Li, Y. Song, C.-X. Zhang, C.-X. Zhao and C. He, *Sep. Purif. Technol.*, 2021, **279**, 119608.